https://doi.org/10.5194/egusphere-2025-230
Preprint. Discussion started: 26 February 2025

Enhanced MOIDS-derived ice physical properties within CoLM revealing bare ice-snow-albedo feedback over Greenland

Shuyang Guo[1], Yongjiu Dai[1]*, Hua Yuan[1], Hongbin Liang[1]

[1] Southern Marine Science and Engineering Guangdong Laboratory (Zhuhai), School of Atmospheric Science, Sun Yat-sen University, Zhuhai, China

Corresponding author: Yongjiu Dai (daiyj6@mail.sysu.edu.cn)

https://doi.org/10.5194/egusphere-2025-230
Preprint. Discussion started: 26 February 2025

Abstract

Under global warming, the Greenland Ice Sheet (GrIS) is experiencing unprecedented mass loss . A key factor closely associated with this loss is the change of snow and ice albedo, which is directly influenced by the firn metamorphism. To investigate the impact of bare ice microstructure changes on the regional warming of the GrIS ablation zone, SNICAR-ADv4 (Snow, Ice and Aerosol Radiation model Adding-Doubling Version 4), a physically based radiative transfer model, is incorporated in Common Land Model version 2024 (CoLM2024). It allows the land surface model represent the ice albedo with changes in ice properties rather than using a constant ice albedo value. Meanwhile, quality control was performed on the bare ice physical property dataset input into CoLM, with multiple MODIS products combined. Using SNICAR-ADv4 reduced the overestimation of shortwave broadband albedo by 60%, with a bias of only 0.053. Further sensitivity experiments indicate that the albedo in the bare ice region is reduced by 0.032 during the summer due to the bare ice metamorphism, producing a 2-m temperature forcing of 0.071°C and a snow cover change of -0.011. The contraction of snow cover exposes more bare ice and will further decrease albedo and increase the ground's absorption of solar radiation, suggesting a feedback mechanism involving bare ice, snow, and albedo. This highlights the indispensable role of bare ice physical properties in the bare ice-snow-albedo feedback for amplifying melt, and more significant feedback is expected to be produced by land-atmosphere coupling model.

Keywords

Greenland Ice Sheet; Bare ice region; Ice albedo; Albedo feedback; MODIS; Remote sensing

1. Introduction

The Greenland Ice Sheet (GrIS), the last remnant of the Ice Age has been melting at a rapid pace since the 1990s, losing around 255 Gt of ice annually in 2003-2016 (Sasgen et al., 2020; Li et al., 2022; van den Broeke et al., 2017). The negative mass balance of the GrIS and peripheral glaciers is the most significant cryospheric factor driving sea level rise, contributing over 25% of observed global sea level rise (Chen et al., 2017; Ryan et al., 2019). Such melting was linked to a combination of processes including climate warming, reduced retention capacity of firn and lower surface albedo (Hofer et al., 2017; King et al., 2020; Ryan et al., 2024). The total mass loss from GrIS consists of two components: surface runoff and frontal ablation occurring at the terminus of outlet glaciers (Cogley et al., 2011, Kochtitzky et al., 2023). Surface losses have exceeded frontal losses in contributing to GrIS mass loss since 2000, with 55% of Greenland's total mass loss attributed to surface mass balance and 45% to the discharge of outlet glaciers between 2000-2018 (Mouginot et al., 2019).

Ice discharge on the surface of the GrIS is partially regulated by the surface albedo. It serves as a fundamental parameter in controlling the absorption of insolation by the ice sheet (Box et al., 2012; Naegeli et al., 2017, Feng et al., 2024). A minor change in snow and ice surface albedo can exert a substantial effect on the energy budget of regional surface-air system, causing significant fluctuations in the energy flux on the surface of the GrIS (Nolin and Stroeve, 1997). Surfaces with high albedo, such as fresh snow, efficiently reflect solar radiation, whereas darker areas, such as glacier ice, absorb the majority of incoming shortwave energy (Whicker et al., 2022). Snow and ice albedo varies with the spatial distribution of snow, ice, and biotic and abiotic light absorbing constituents (LACs) and further evolves with the melting of snowpack and glacier surfaces through the spring and summer. Fluctuations in the snowline dictate the relative extend of dark bare ice and brighter snow (Ryan et al., 2019), and GrIS's surface melt can be attributed to the exposure of bare ice (Antwerpen et al., 2022) and the processes that darken bare ice itself (Chevrollier et al., 2023). Dark bare ice extent closely tracks interannual variations in snowline elevation and was exposed as the snowline retreats further inland during the melt season, leading to the reduction of ice sheet albedo and the intensified melt. This positive feedback has been referred to as the "snow-albedo feedback" (Ryan et al., 2019).

In the preceding decades, polar amplification has contributed to the progressive darkening of the GrIS and the prolongation of the melt season, both of which serve as positive feedback mechanisms that intensify surface melt (Tedesco et al., 2016). As the warming occurs in the ice surface, bare ice albedo is reduced through melt processes that darken the ice surface. Notably, these processes include exposure of dust layers, pooling of surface meltwater, increased interstitial water content, and liquid meltwater-induced growth of pigmented ice algal assemblages that inhabit the bare ice surface (Cook et al., 2020; Stibal et al., 2017; Tedstone et al., 2020; Williamson et al., 2018; Whicker et al., 2022). Despite operating over a relatively small area of the ice sheet, it is argued that these bare ice processes have contributed substantially to an observed reduction in albedo and associated increase in melt across GrIS's ablation zone from 2000 to 2011 (Stibal et al., 2017; Tedstone et al., 2017). This category of physical and biological melt-albedo processes that darken bare ice is referred as the "bare ice-albedo feedback" (Ryan et al., 2019). However, the complex and non-linear response of regional snow and ice, particularly in ablation zones, to changes in meteorology and climate highlights the growing necessity to model these surfaces using physical principles rather than relying solely on empirical methods (Box et al., 2012). Therefore, accurately modeling the influence of snow and ice on the albedo of the GrIS becomes increasingly important to capture these dynamics effectively.

The albedo of the cryosphere varies widely depending on the solar zenith angle (SZA), atmospheric conditions, metamorphic state of the snow and ice, and impurities (He and Flanner, 2020). The Snow, Ice, and Aerosol Radiative (SNICAR) model is one of the most widely used snowpack radiative transfer models (Flanner et al., 2021). Initially, it combined the theory from Wiscombe and Warren (1980) and Warren and Wiscombe (1980) with the multi-layer two-stream solution from Toon et al. (1989) to enhance the simulation of snow albedo (Flanner et al., 2007). Updates and new features have also been incorporated within SNICAR, including eight species of LACs (Flanner et al., 2007), four snow grain shapes (He et al., 2018), black carbon-snow and dust-snow internal mixing state (Flanner et al., 2012; He et al., 2017, 2019). Dang et al. (2019) developed SNICAR-AD by substituting the tri-diagonal matrix solution solving method (Toon et al., 1989) with the delta-Eddington adding-doubling radiative method, as a result of the latter's superior computational stability across varying solar zenith angles and higher computational efficiency (He et al., 2024). To represent ice albedo, Whicker et al. (2022) further developed SNICAR-ADv4 by integrating and extending key features from earlier radiative transfer models to achieve more accurate simulations of a spectrally resolved cryospheric column of snow and ice with a refractive boundary, while incorporating light-absorbing constituents (LACs), such as black carbon (BC) and algae, into this offline radiative transfer model. It simulates bare ice using the physical microscopic structure of the ice, including the ice density, the scattering air bubbles within an absorbing ice medium, and a refractive boundary that depicts the refraction across snow-ice interfaces (Briegleb and Light, 2007; Gardner and Sharp, 2010; Mullen and Warren, 1988).

Nevertheless, the ice albedo is typically prescribed as a constant value in the visible (VIS) and near-infrared (NIR) spectral regions in Earth system models (ESMs). For instance, Ice albedo is 0.6 in the visible and 0.4 in the NIR in the default version of the Energy Exascale Earth System Model (E3SM) and the Community Earth System Model (CESM) version 2 (Whicker et al., 2024). Such parameterization does not capture the albedo of solid ice or variations in spectral albedo with changing ice conditions. To advance ice radiative transfer modeling in Earth system models (ESMs), Whicker et al. (2024) incorporated SNICAR-ADv4 into the E3SM, in which the GrIS ice physical properties are retrieved by the satellite observation data. This enhancement enables more realistic simulations of the GrIS bare ice albedo, and concurrently reveals that the default ELM method overestimates bare ice albedo by 4% in the visible and 7% in the NIR bands. However, the quality information of MODIS albedo products were not considered in the process of acquiring bare ice properties in their study. Schaaf et al. (2011) noted that the MODIS poor-quality inversions beyond a SZA of 70° are characterized by high noise and often significantly lower than the more stable and consistent values observed at smaller SZAs. Omitting quality flags could, therefore, lead to an underestimation of Greenland's snow/ice albedo and introduce significant uncertainties in the retrieval of bare ice physical properties. Despite the aforementioned modeling advances, the Common Land Model (CoLM) still uses fixed values to represent ice albedo (0.80 in the visible and 0.55 in the NIR). For the purpose of investigating the impacts of bare ice metamorphism under polar warming, it is also imperative to incorporate ice radiative transfer techniques into CoLM to enhance albedo modeling with more realistic and physical representations of snow-ice-LAC-radiation interactions.

In this study, we focus on the bare ice region of the GrIS, characterized by the presence of land ice, and bare ice is exposed with snow melting in ablation season. The aim of this study is to develop a more reliable dataset of Greenland's bare ice physical properties by incorporating the quality information of MODIS albedo products, and explore the bare ice-albedo feedback associated with the metamorphism of bare ice after the implementation of the SNICAR-ADv4 into the CoLM. This paper is organized as follows. Section 2 provides descriptions of the CoLM snow and ice albedo schemes and details the model simulations, as well as the explanation of the use of various MODIS products to inform the ice albedo calculations in SNICAR-ADv4. Section 3 compares the differences in albedo simulations with and without ice radiative transfer solver (SNICAR-AD and SNICAR-ADv4), and quantified the impact of varying bare ice propertyies on the near-surface air temperature and the snow cover. Section 4 is conclusions and discussion.

2. Models, Data, and Methods

2.1 CoLM Snow and Ice Albedo Scheme

The CoLM version 2024 (CoLM 2024) used in this study is based on the CoLM 2014 and features enhancements to surface energy, hydrology, biogeochemical cycles, and anthropogenic disturbance processes. The available snow albedo schemes of the CoLM 2024 are BATS (Dickinson et al., 1986) and SNICAR-AD (Dang et al., 2019). For ice albedo, the CoLM uses fixed values of 0.80 in the visible and 0.55 in the NIR. As one of the representative snow albedo schemes, BATS is simply computes snow surface albedo for direct and diffuse radiation over visible and NIR spectrums with snow age, surface temperature, solar zenith angle (SZA), and absorptive impurities (Abolafia-Rosenzweig et al., 2022). SNICAR-AD is another snow albedo scheme embedded in the CoLM 2024 used to compute snow albedo for the multi-layer (up to 5 layers) snowpack with the two stream radiative transfer scheme of the delta-Eddington approximation and adding-doubling technique, accounting for the effects of snow grain size and LAC contamination on snow albedo. It uses the physical properties of the snowpack and albedo of the top layer of the underlying ground to determine the column albedo (Flanner and Zender, 2006). The input variables for SNICAR-AD consist of direct and diffuse radiation, the surface downward solar spectrum, the solar zenith angle (for direct radiation), the ground albedo beneath the snowpack, vertical profiles of snow grain size, snow layer thickness and density, aerosol concentrations of each snow layer, as well as the optical properties of both snow and aerosols.

To achieve better albedo simulation using the satellite-informed ice microphysical properties and to explore the regional climatic response induced by changes in bare ice albedo, we implement the SNICAR-ADv4 into the CoLM. Then, using SNICAR-AD or SNICAR-ADv4 becomes an adjustable switch and both have the same radiative transfer solver to calculate snow albedo, with the only difference being in how they obtain ice albedo. In other words, using CoLM SNICAR-ADv4 enables the simulation of radiative processes over both ice and snow surfaces. For snow albedo modeling, CoLM SNICAR-ADv4 has been updated to include snow nonsphericity, BC/dust-snow internal mixing (Hao et al., 2023), contributing to improved simulations of snow surface energy and water balances. For ice albedo modeling, as proposed by Whicker et al. (2024), the radiation transfer process within the ice layer can be calculated in the land surface model, which requires input variables such as ice density, air bubble effective radii within the ice, equivalent BC concentrations, and downward solar spectra. The need for air bubble parameters arises from the representation of ice layers as collections of independently scattering air bubbles within a solid ice medium in SNICAR-ADv4, while snow layers are treated as independently scattering ice crystals in an air medium (Picard et al., 2016; Whicker et al., 2022).

2.2 Model simulation

We conduct several land-only CoLM simulations on a 0.5×0.5-degree resolution driven by

https://doi.org/10.5194/egusphere-2025-230
Preprint. Discussion started: 26 February 2025

the atmospheric forcing from the 6-hourly European Center for Medium-Range Weather Forecast's fifth-generation atmospheric Reanalysis (ERA5) in the GrIS. Compared with other atmospheric forcings, ERA5's precipitation rates exhibit a higher correlation with measured net accumulation over the GrIS (Schneider et al., 2023). We run the model simulations for the years 1980–2020 and the summer melt season (June, July and August; JJA) during 2000-2020 is used for analysis. Aerosol concentration in the snow layer is calculated based on the prescribed monthly aerosol (BC, dust, OC) wet and dry deposition flux from the CESM2-WACCM simulations participated in CMIP6 experiments (Danabasoglu et al., 2020). The monthly bare ice properties for ice radiative transfer process are inferred from MODIS products over the bare ice region of the GrIS, covering the JJA from 2000 to 2020, as the MODIS products has been available since 2000. To prevent possible unusual model behavior when shifting bare ice albedo schemes, the bare ice properties from the summer of 2000 were used in a brief spin-up run for the variable bare ice conditions in our experimental runs from 1998 to 2000. For land ice patches informed by the ice properties, the bare ice albedo is first calculated and replaces the constant values (0.8 for VIS and 0.55 for NIR). If snow is present over the ice, the new ice albedo of underlying ice column is used as the lower boundary to calculate snow albedo. The total patch albedo is then determined by the fractional coverage of land types and snow cover.

2.3 Data

The MODIS land cover data (MCD12C1) is used to remove grids that are not classified as snow or ice. The selected MCD12C1 Version 6.1 dataset has a spatial resolution of 0.05°×0.05° and annual intervals (Friedl et al., 2010). MODIS MCD43C3 product is extracted during the summer melt seasons of 2000-2020 to evaluate the simulation of the albedo in GrIS bare ice region. MOD09CMG reflectance product (Vermote 2021), along with MCD43C3 (Schaaf and Wang, 2021), is used to retrieve the optically relevant physical properties of bare ice surfaces. The daily MCD43C3 albedo data provides spectral (MODIS bands 1 to 7) and broadband (VIS 0.3–0.7 μm, NIR 0.7–5.0 μm and shortwave 0.3–5.0 μm) black-sky albedo (BSA) and white-sky albedo (WSA) at local solar noon, by using 16 days of

Aqua-Terra merged surface albedo dataset based on the bidirectional reflectance distribution function (BRDF) algorithm (Schaaf and Wang, 2021). Among the GLASS-AVHRR and C3S-v2 albedo products, MCD43C3 stands out as the most reliable for monitoring snow albedo, exhibiting the lowest bias and RMSE over snow and consistent performance across diverse snow cover conditions (Urraca et al., 2022). In the GrIS, MCD43A3 was found to outperform the GLASS albedo product and even the reconstructed albedo based on the MOD10A1, for the sites located in the GrIS ablation zone (Ye et al., 2023).

Considering the little difference between BSA and WSA for a typical summer day, using BSA is considered acceptable for analyzing the GrIS during the summer (Alexander et al., 2014; Stroeve et al., 2005). For MODIS MCD43C3 product, we use its SZAs and the MCD43A3 BSA band 2 (0.841–0.876 µm), visible, NIR and shortwave albedo. Figure 1a shows the daily variation of the regionally weighted average SZA over Greenland from May to September, and the period during which the SZA>70° is primarily concentrated in September. For the relationship between the SZAs of MCD43C3 and their spatiotemporally corresponding albedo quality index (Figure1b), it can be seen that the percentage of low-quality indices (4 and 5) rises drastically as the SZA increases at higher SZA. Therefore, we excluded albedo values identified with a low-quality index when the SZA exceeded 70° to make more reliable satellite-retrieved bare ice physical properties.

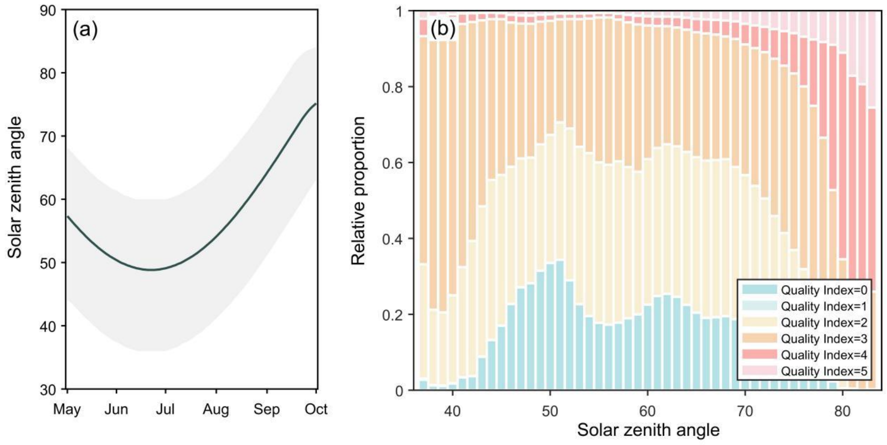

Figure 1. Regional-weighted mean SZAs of Greenland at local noon from May to September

https://doi.org/10.5194/egusphere-2025-230
Preprint. Discussion started: 26 February 2025

(a; solid line). Grey shaded area represents the range of SZAs over Greenland. Relative proportion of the quality index of MCD43C3 albedo dataset under different SZAs over Greenland during May to September (b; 0 for best quality and 5 for poorest quality)

2.4 Method

The method described by Whicker et al. (2024) for obtaining ice physical properties (ice density, air bubble effective radius and equivalent BC) from MODIS bare ice albedo involves two main steps. First, a GrIS bare ice mask and cloud mask are created using MODIS data to identify bare ice areas without cloud cover. Second, the bare ice physical properties are retrieved using MCD43A3 band 2 BSA and SZA, based on a lookup table generated by the 480-band offline SNICAR-ADv4 model. For the fist step, the MOD10C1 cloud mask is applied to exclude cloud-covered pixels, while a bare ice mask is used to remove snow-covered pixels (Antwerpen et al., 2022). The spectral reflectance of snow and bare ice in a MODIS image signifies that snow surface reflectance is significantly higher than that of bare ice, particularly at a wavelength of 0.86 µm (Shimada et al., 2016). Thus, bare ice pixels are identified by applying a threshold of 0.6 to band 2 (841–876 nm) in the MOD09CMG product (Antwerpen et al., 2022; Whicker et al., 2024). Additionally, the NIR region of the spectrum is useful for determining the physical properties of bare ice, as it is sensitive to changes in snow and ice microphysical properties and is minimally affected by surface LACs (Schneider et al., 2019). The resulting bare ice extent is then filtered to exclude pixels with elevations exceeding the mean equilibrium line altitude of 1679 m a.s.l. (Antwerpen et al., 2022). Then, we upscale the filtered MODIS product from a spatial resolution of 0.05°×0.05° to 0.5°×0.5°.

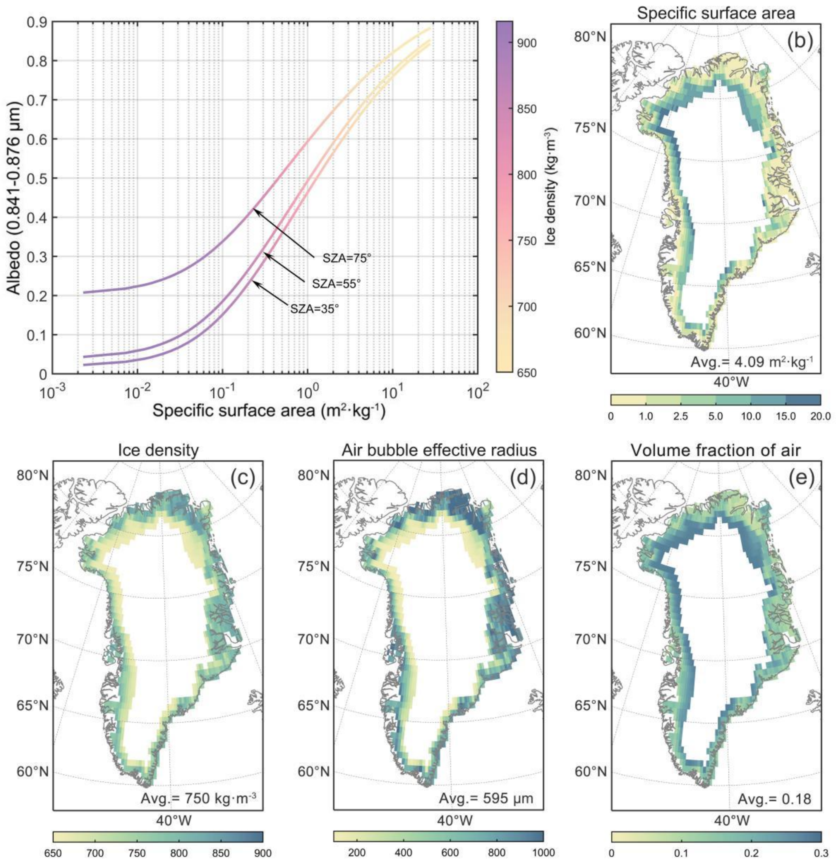

Figure 2. MCD43C3 band 2 (0.841-0.876 µm) albedo as a function of ice specific surface area (SSA) and solar zenith angle (a). Spatial distribution of JJA (b) specific surface area ($m^2 \cdot kg^{-1}$), (c) ice density ($kg \cdot m^{-3}$), (d) air bubble effective radius (µm) and (e) volume fraction of air in the period of 2000-2020.

The lookup table was generated by running offline SNICAR-ADv4 simulations. Considering that ice can be classified as cryospheric media with densities exceeding 650 $kg \cdot m^{-3}$, in optimal agreement with measurements, and that the local noon solar zenith angles (SZAs) for CoLM GrIS grid cells over the GrIS range from 35° to 75°, We adjusted the input parameters, including ice densities from 650 to 916 kg/m^3 and air bubble effective radii from 100 to 1500 µm, for each SZA within the 35°–75° range. The band 2 albedo, specific surface area (SSA) and the volume fraction of air (V_{air}) included were then output by the offline SNICAR-ADv4.

The relationship between the SSA (α, units: $m^2 \cdot kg^{-1}$) and ice density and ari bubble effective radius is given by Eq.1, where ρ_{blk} is layer bulk ice density used to calculate the volume fraction of air (Eq.2). Figure 2a shows the band 2 albedo from the SNICAR-ADv4 lookup table as a function of SSA, a measure of the total surface area of ice-air interfaces relative to the ice mass. It is noteworthy that there is a one-to-one relationship between SSA and albedo for a given SZA, while the relationship between SSA, ice density, and air bubble radius is not unique. Since MCD43C3 provides the band 2 albedo and SZA for each bare-ice grid cell, the corresponding bare ice physical properties can be inferred from the lookup table.

$$\alpha = \frac{3V_{air}}{\rho_{blk} R_{eff}} \qquad \text{(Eq. 1)}$$

$$V_{air} = \frac{\rho_{ice} - \rho_{blk}}{\rho_{ice}} \qquad \text{(Eq. 2)}$$

After acquisition of the daily ice density and air bubble effective radius of the GrIS (Figure 2c and 2d), we again employed the offline SNICAR-ADv4 model to simulate the NIR and visible albedo for each bare ice grid cell of the GrIS. This allowed us to obtain the equivalent black carbon concentration by comparing the bare ice visible albedo from the offline SNICAR-ADv4 with that of the MCD43C3, due to the strong impact of LACs on visible albedo and negligible effect on NIR albedo for the bare ice (Schneider et al., 2019). As seen in Figure 3a-c, there is minimal difference in the albedo in the NIR band, with a slight underestimation of 0.029 by the offline SNICAR-ADv4. In contrast, the SNICAR-ADv4 significantly overestimated the visible albedo by up to 0.293 when using these bare ice properties, as it did not account for the LACs (Figure 3d-f). We incrementally increased the input BC concentration in the offline SNICAR model until the simulated visible albedo exactly equaled that of MCD43C3 at each GrIS bare ice grid cell (Figure 3h and 3i), and then, the daily equivalent BC concentration was acquired (Figure 3g). Based on the MODIS data and the offline SNICAR-ADv4 lookup table, the daily 0.5-deg ice density, air bubble effective radius and equivalent BC data were then processed into monthly timescale as input for CoLM. Besides, it is worth mentioning that not all bare ice grid cells are informed by the bare ice physical properties data in each summer month. These grid cells are filled with the climatological mean values of bare ice physical properties excluding the current year.

https://doi.org/10.5194/egusphere-2025-230
Preprint. Discussion started: 26 February 2025

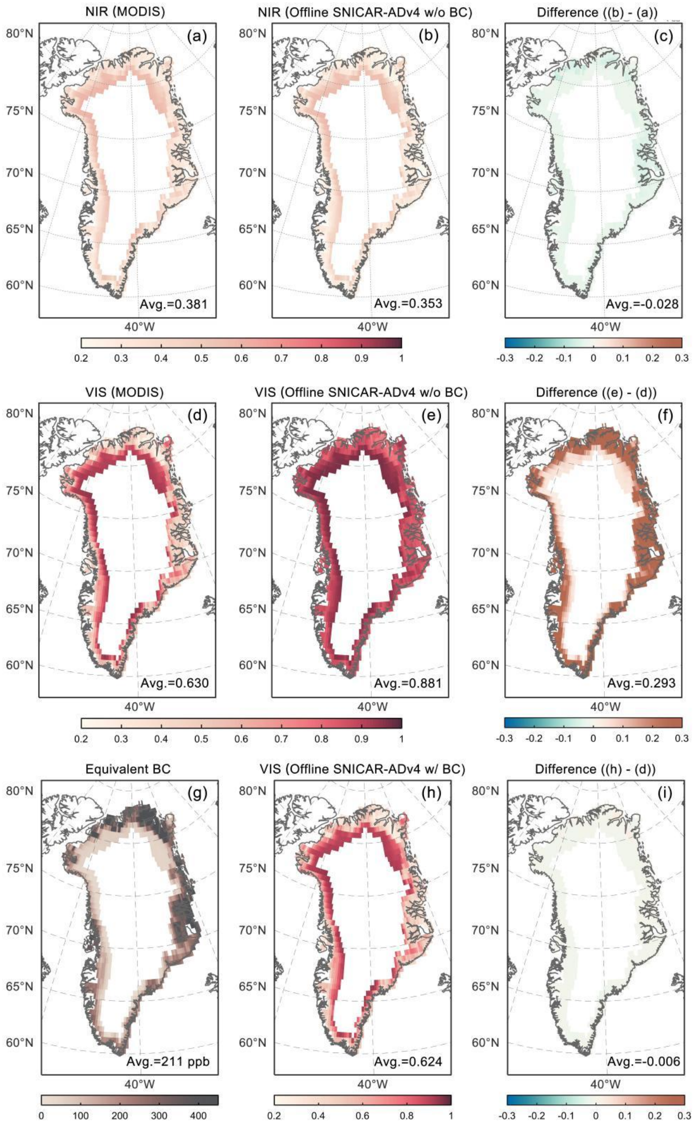
NIR (MODIS)
NIR (Offline SNICAR-ADv4 w/o BC)
Difference ((b) - (a))
VIS (MODIS)
VIS (Offline SNICAR-ADv4 w/o BC)
Difference ((e) - (d))
Equivalent BC
VIS (Offline SNICAR-ADv4 w/ BC)
Difference ((h) - (d))

Figure 3. The spatial distributions of MODIS bare ice albedo and offline SNICAR-ADv4 bare ice albedo excluding LACs in (a, b) near-infrared and (c, d) visible bands for the JJA from 2000 to 2020, along with (c, f) their differences. The spatial distributions of (g) equivalent black carbon, (h) the offline SNICAR-ADv4 bare ice visible albedo with equivalent black carbon (ppb), and (i) its difference from the MODIS bare ice visible albedo.

We use the offline SNICAR-ADv4 and briefly examine aforementioned factors influencing spectral albedo of ice with direct light conditions, including the SZA, ice density, air bubble effective radius (R_{eff}), and equivalent BC. As shown in Fig. 4a, total internal reflection occurs at wavelengths around 3μm for SZA greater than 55°, and the wavelength range for total internal reflection expands with the increases in SZAs. This phenomenon occurs for pure and smooth ice surfaces but is not representative of naturally occurring ice, which typically has impurities and rough surfaces. For the dependency of albedo on ice density, air bubble effective radius, the spectra show that the albedo declines as the ice density and air bubble radius increases since air bubbles within ice are responsible for the scattering light and smaller bubbles scatter light more efficiently in the visible and near-infrared parts of the spectrum (Fig 4b-c). Furthermore, BC impacts ice albedo rather uniformly across the visible spectrum and has almost no impact at λ > 1.0 μm.

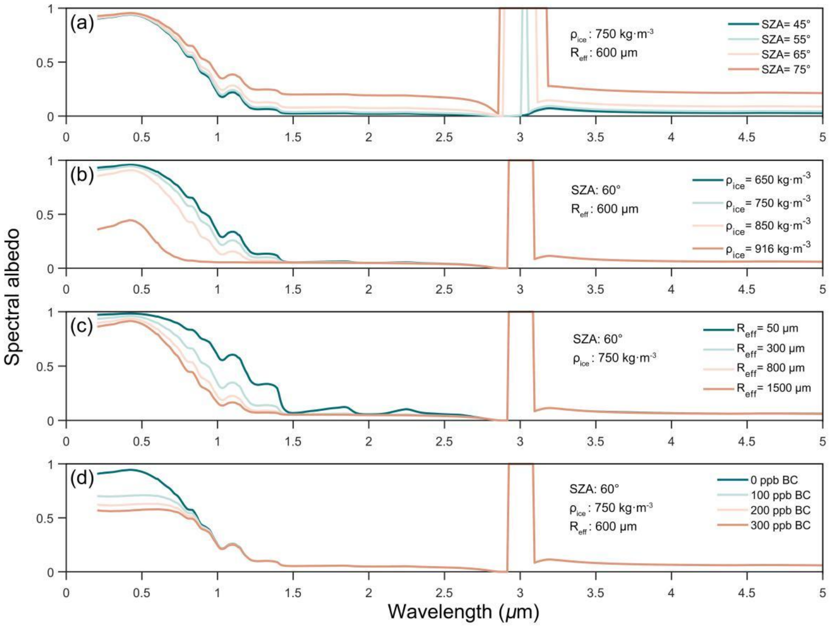

Figure 4. Spectral albedo simulated by offline SNICAR-ADv4 under direct incident irradiance with varing (a) SZA, (b) ice density, (c) air bubble effective radius and (d) BC concentration.

https://doi.org/10.5194/egusphere-2025-230
Preprint. Discussion started: 26 February 2025

3. Results

3.1 Mapping of GrIS bare ice physical properties

Figure 2b-e demonstrate the spatial distribution of summer climatological mean of the bare ice physical properties, including SSA, ice density, air bubble effective radius and volume fraction of air. The bare ice density gradually decreases from the lower-elevation coastal regions toward the interior, while the volume fraction of air show an opposite pattern for it is calculated by bulk ice-air mixture density and pure ice density (Figure 2c and 2e). SSA represent the total surface area of ice-air interfaces relative to the mass of ice, determined by the volume fraction of air, effective diameter of air bubbles, and the bulk density of the ice layer (Whicker et al., 2022), with high-value area distributed in the area along the mean equilibrium line (Figure 2b). Given the large discrepancy in bare ice visible albedo between the offline SNICAR-ADv4 without LACs and the MCD43C3 in the coastal regions of the GrIS (Figure 3d and 3e), there are higher concentrations of equivalent BC in these areas compared to those farther inland, indicating potentially more severe contamination, particularly in the southwest, east, and northernmost parts of the GrIS (Figure 3g).

3.2 Spatial and Temporal performance of CoLM Simulations

The bare ice region of the GrIS in this study is defined as the grid cells containing land ice that are not entirely covered by snow, emphasizing the joint effect of ice and snow on the albedo. Figure 5a illustrated the spatial distribution of the fraction of land ice underlying snowpack, and areas with land ice as the primary land cover type are mainly located in the southwestern and northeastern GrIS, which means these grid cells may also contain other land cover type, e.g. bare soil. In tandem with the effect of snow cover simulated by SNICAR-ADv4 enabled CoLM, the exposed bare ice fraction (Figure 5b) is calculated accounting for the snow coverage in each grid cell, utilizing the SNICAR-AD scheme. It is important to note that, despite a slight difference in snow cover fraction simulations, the choice of snow albedo scheme does not affect the selection of bare ice regions. The exposed bare ice fraction frequency distribution is shown in Figure 3d, in which the bare ice fraction spans from 0 to 0.7, and in most areas, the bare ice fraction is less than 0.5.

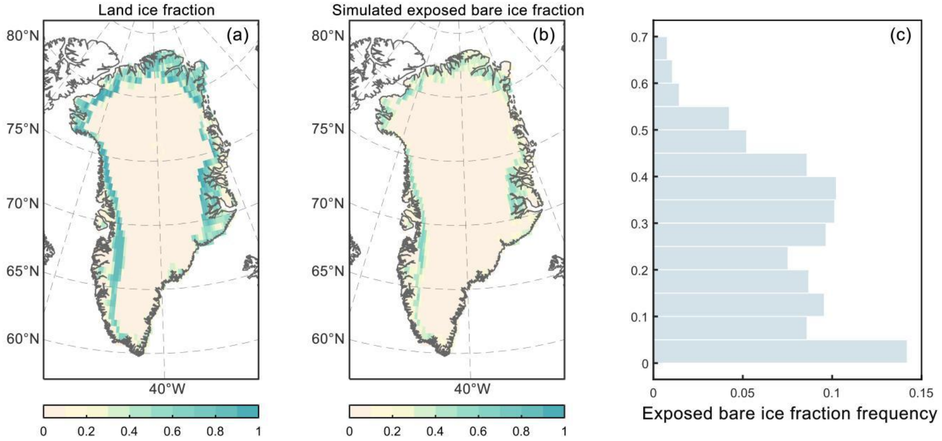

Figure 5. Spatial distribution of (a) the fraction of land ice underlying snowpack and (b) exposed bare ice considering the snow cover simulated by SNICAR-ADv4 enabled CoLM for the JJA from 2000 to 2020. Frequency distribution of exposed bare ice in the bare ice region (c; excluding grid cells with no exposed bare ice).

To assess whether the integration of an ice radiative transfer solver in CoLM improves albedo simulations, we compared simulated albedo with the MCD43C3 albedo in shortwave, visible and NIR regions of the spectrum during the summer of 2000-2020 in bare ice region (Figure 6). Both schemes of SNICAR-AD and SNICAR-ADv4 maintain consistent settings for default snow albedo scheme, with sphere snow grain shape, adding-doubling radiative transfer solver, and BC/dust-snow external mixing state. In other words, the differences in albedo simulated by these two schemes are determined by the treatment for ice albedo. As seen in Figure 6d-f, it is obvious that the SNICAR-AD enabled CoLM albedo is significantly overestimated across all bare ice region, by 0.132 in shortwave, 0.131 in visible and 0.132 in NIR. Compared with CoLM SNICAR-AD, the application of the SNICAR-ADv4 scheme reduced the overestimation of albedo for all bands, by 60% in the shortwave, 70% in the visible and 48% in the NIR (Figure 6d-i). Furthermore, the CoLM SNICAR-ADv4 albedo demonstrates superior performance compared to the CoLM SNICAR-AD albedo in terms of

https://doi.org/10.5194/egusphere-2025-230
Preprint. Discussion started: 26 February 2025

correlation coefficient and root mean square error (RMSE) valuation metrics, as well as linear trend (Figures S1-S3).

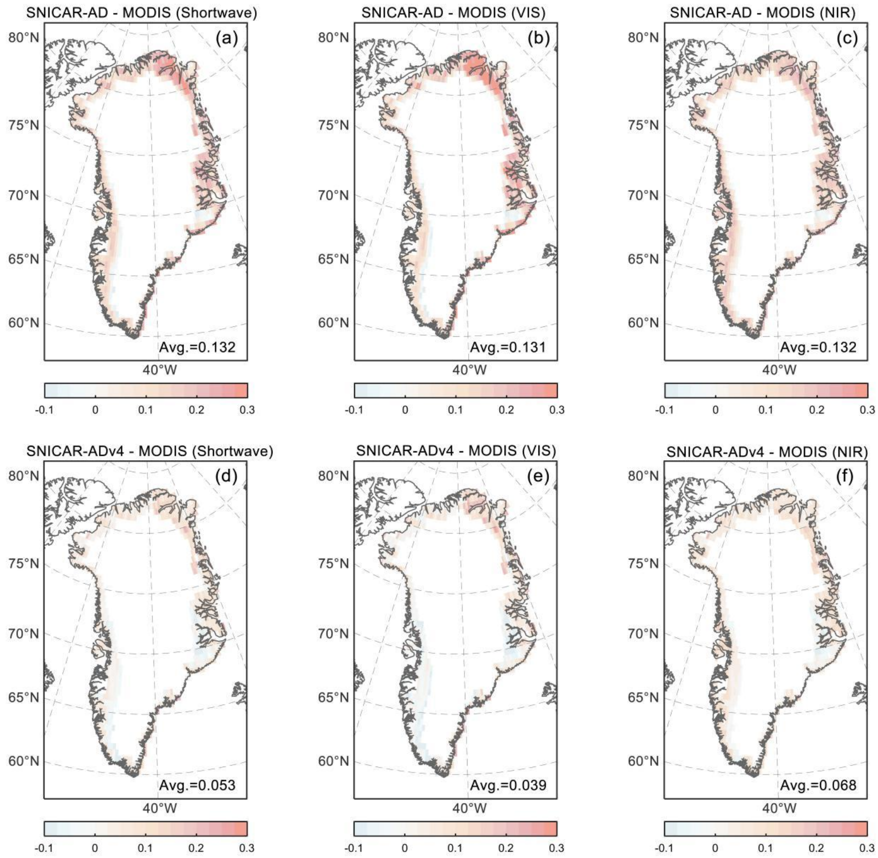

Figure 6. Spatial distribution of the difference of the 2000-2020 JJA albedo between the CoLM with different snow/ice albedo schemes (SNICAR-AD and SNICAR-ADv4) and the MCD43C3 in the (a, d) shortwave (0.3–5.0 μm), (b, e) visible (0.3–0.7 μm) and (c, f) near-infrared (0.7–5.0 μm) bands.

Temporally, the decrease in positive bias of CoLM SNICAR-ADv4 can be also clearly witnessed in the time series of shortwave, visible and NIR albedo, with the consistent lower area-weighted average albedo of GrIS bare ice region in all summertime from 2000 to 2020, by comparing it to that of CoLM SNICAR-AD (Figure 7). The albedo of CoLM SNICAR-ADv4 fluctuates around 0.47 in the shortwave, 0.53 in the visible, and 0.4 in the

NIR, which is approximately 0.05 higher than the corresponding values in MCD43C3. In addition, the SNICAR-ADv4 enabled simulations exhibit synchronous variations in albedo with those of MCD43C4, and there are relatively high temporal correlations between the CoLM SNICAR-ADv4 and MCD43C4 albedo, with the values up to 0.95 for the shortwave, visible, and NIR bands. In contrast, the albedo from the CoLM SNICAR-AD shows lower correlation with MCD43C3 due to its constant ice albedo treatment. It is obvious that a large interannual variability in the SNICAR-ADv4 enabled CoLM albedo is in consistence with that of the MCD43C3, while the simulated albedo using SNICAR-AD scheme present a weaker interannual variability. Besides, the SNICAR-AD albedo demonstrates a lower correlation of 0.71 in the NIR but higher correlations with the MCD43C3 albedo of 0.91 and 0.90 in the shortwave and visible, respectively (Figure 7).

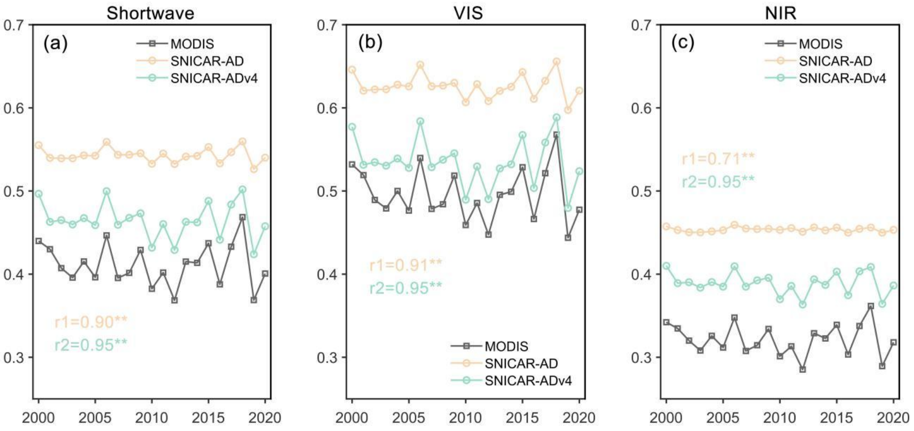

Figure 7. Time series of the 2000-2020 JJA CoLM SNICAR-AD and SNICAR-ADv4 albedo versus the MCD43C3 albedo over bare ice region, in the (a) shortwave (0.3–5.0 μm), (b) visible (0.3–0.7 μm) and (c) near-infrared (0.7–5.0 μm) bands. Double asterisks indicates significance at the 99% confidence level.

Given that the bias reduction varies across regions with different bare ice coverages, we explore the distribution of the albedo from CoLM SNICAR-AD, CoLM SNICAR-ADv4 and MCD43C3 under different bare ice fractions. Generally, as bare ice fraction increases, CoLM SNICAR-ADv4 can more effectively reduce the overestimation of shortwave broadband albedo (BBA) from CoLM SNICAR-AD, due to its improved simulation of bare ice BBA (Figure 8). For regions where bare ice covers more than half the area, the albedo overestimation of SNICAR-AD was reduced significantly by up to 99%. When the bare ice fraction is between 0.4 and 0.5, the percentage of overestimation reduction in albedo decreases to 88%, followed by regions with bare ice fraction of 0.3-0.4 (70%), 0.2-0.3 (57%), 0.1-0.2 (42%), and 0-0.1 (20%), respectively.

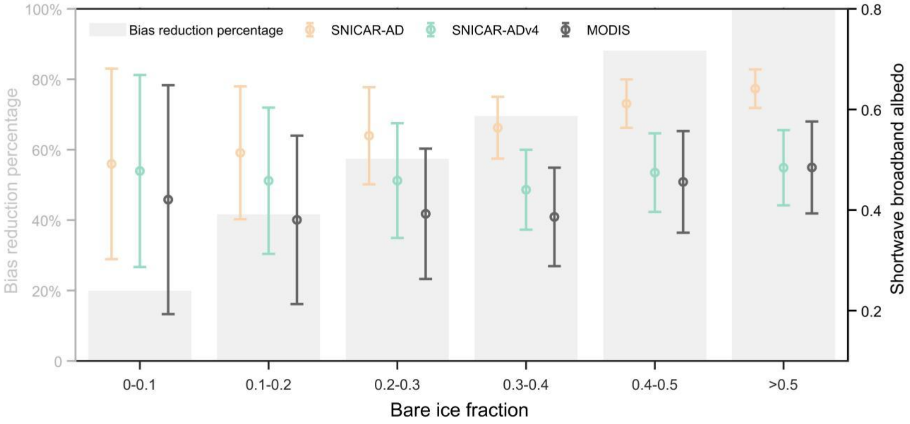

Figure 8. Mean shortwave broadband albedo from CoLM SNICAR-AD, CoLM SNICAR-ADv4 and MCD43C3 under different bare ice fractions (error plots). The uncertainty is calculated as double standard error, which reflects the 95% confidence interval. The percentages of CoLM SNICAR-ADv4 albedo reduction in bias are represented by grey bars.

3.3 A feedback revealed by bare ice properties change

The application of the SNICAR-ADv4 scheme in CoLM significantly has reduced the bias in albedo simulations. To investigate the regional climatic response to bare ice metamorphism of Greenland's bare ice region, we conduct a simulation in which the bare ice physical properties for each year are set to the values from 2000. By calculating the difference in simulated albedo between the simulations with annually varying bare ice properties and those using the 2000 values, the model sensitivities to the change in summer bare ice albedo can be assessed to quantify its impact on 2-m temperature and snow cover. To better highlight the impact of changes in bare ice physical properties, the study area was restricted to regions with a bare ice fraction larger than 0.4. Figure 9a shows the effects of bare ice metamorphism on the 21-year annual mean albedo, 2-meter temperature, and snow cover fraction when using annually varying bare ice properties compared to the 2000 baseline values. The regional weighted mean albedo difference between the two experiments reaches 0.032, indicating that the albedo in the bare ice region is reduced by 0.032 during the summer due to bare ice metamorphism. This leads to a 0.071°C 2-meter temperature forcing and a -0.011 change in snow cover fraction over the study period (Figure 9d). These results suggest that the temperature increase associated with the change in albedo contributes to snow melting.

Spatially, the regions with strong response of near surface air temperature to bare ice albedo changes are concentrated in the edge of the northeast ablation zone, where the 2-temperature increased by over 0.1°C in most part of these areas (Figure 9b). A similar response pattern can be also seen in the difference distribution of the snow cover (Figure 9c), with decrease in snow cover fraction exceeding 0.04 in parts of the northeastern GrIS due to the significant warming. Such response of the temperature and snow cover manifest a strong bare ice-albedo feedback in the GrIS bare ice region because bare ice albedo is reduced through physical and biological melt-albedo processes that darken the ice surface as the warming occurs in the ice surface. The metamorphism of bare ice could be manifested in the changes in the ice density and air bubble radius with the ice, and these two factors jointly determine the specific surface area (Eq.1) which have one-to-one relationship with the bare ice albedo (Figure 2a). From Figure 9d, the difference in BBA shows a strong positive correlation with the specific surface area, with a correlation coefficient of 0.88 (significant at the 99% confidence level), since the control experiment only altered the bare ice physical property data input into the land surface model. As more intense melt processes commence in the early summer of the GrIS ablation zone after 2000, the lower specific surface area, linked with the bare ice-albedo feedback, consistently contributes to the reduction of the BBA (Figure 9d). Additionally, according to the sensitivity of modeled spectral albedo to the relevant parameters of the offline SNICAR-ADv4 model (Figure 4), the decreased bare ice albedo, associated with a lower specific surface area, suggests an overall increase in ice density and a larger size of air bubbles within the ice in the GrIS bare ice region.

After 2000, the metamorphism of bare ice in the Greenland bare ice region is mainly reflected in the decrease of SSA, which leads to ice darkening. This, in turn, induces region near-surface temperature increases, causing snowmelt and ultimately resulting in a reduction of snow cover. Changes in snow cover directly determine the extent of bare ice exposure and significantly effect the albedo through snow-albedo feedback. The obvious snow cover contraction attributed to the changes in the physical properties of bare ice will cause more dark ice exposure and darkening, and make a constant contribution to albedo reduction in this ablation zone, suggesting a potential linkage between the bare ice-albedo and the snow-albedo feedback.

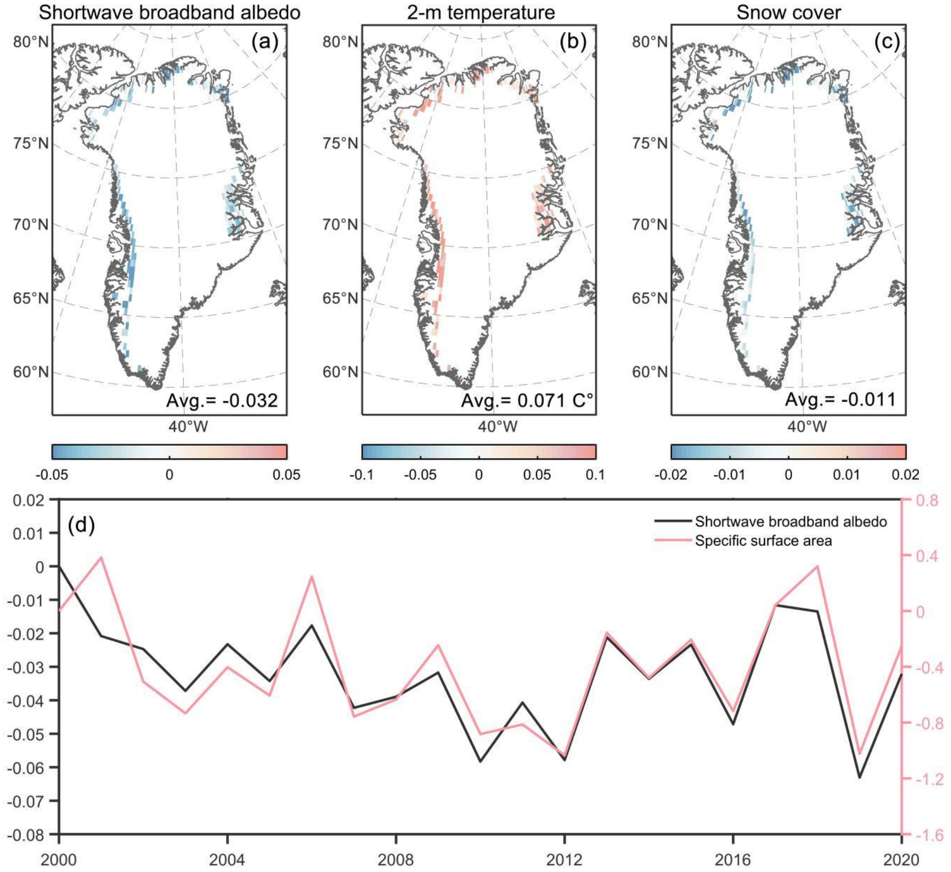

Figure 9. Spatial distribution of the differences between the simulations using annually varying bare ice properties and those using the 2000 values in 2000-2020 JJA (a) albedo, (b; units:°C) 2-m temperature and (c) snow cover. Time series of the differences in speciafic surface area (units: $m^2 \cdot kg^{-1}$) and simulated shortwave broadband albedo between the two experiments (d).

4. Conclusions and Discussion

In this study, we incorporated SNICAR-ADv4 into the CoLM and made an enhanced MODIS-informed bare ice physical properties to explore the response of the bare ice albedo to the ice metamorphism under polar warming. The use of SNICAR-ADv4 in CoLM significantly reduces the severe overestimation originated from the default ice albedo treatment, with the improvement of the albedo modeling by 60%, 70% and 48% for the BBA, visible and NIR albedo. The snow and ice treatment used in CoLM SNICAR-ADv4 schemes, and SNICAR-AD are summarized in the Figure 10, and it is evident that SNICAR-ADv4 performs radiative transfer calculations not only over the snow column but also over the ice column. During the summertime of 2000-2021, the bare ice BBA decreased by 0.032 due to the changes in bare ice physical properties. The subsequent darkening of the bare ice led to a 2-m air temperature forcing of 0.071°C and a change in snow cover of -0.011 over the 21-year period, suggesting that even a slight reduction in bare ice albedo can trigger strong climate responses in ablation region.

Our findings highlight the impact of bare ice-albedo feedback associated with bare ice properties changes summarized in Figure 10, where a drastic contraction of snow cover occurred because of the reduction in bare ice albedo in ablation zone, leading to more bare ice exposed and subsequent regional albedo reduction, especially in the northern GrIS. This is consistent with previous research, suggesting that increased bare ice exposure in North Greenland will intensify the impact of the GrIS snow-albedo feedback, with its strength rising by 51% in their 2001–2017 study period (Ryan et al., 2019). Although the hydrological and biological processes that darken bare ice, including algae growth, exposure of impurities and interstitial water, have been found to be the secondary contributor to amplifying ice sheet melt up in the period of 2001-2017, relative to the processes that expose bare ice (Ryan et al., 2019), the changes of bare ice properties were an important control on ice sheet meltwater quantities in GrIS, which decrease the snow cover to some extent and will further leverage the effect of snow-albedo feedback. Meanwhile, rising temperatures may alter the microphysical properties of bare ice, leading to a further decrease in its albedo. It is noteworthy that the bare ice-albedo feedback in this study refers to the changes in bare ice physical properties, characterized by a downward trend in specific surface area of -0.007 yr^{-1}, albeit statistically insignificant. Thus, we collectively term these processes of the variation in the bare ice albedo associated with snow melting the bare ice-snow-albedo feedback (Figure 10). Such feedback is anticipated to drive an increase in the frequency of glacier calving, surface ablation, submarine and subaerial melting in the GrIS bare ice region, and these possible intensification of glacier responses present a valuable avenue for future research.

This study advances our understanding of the performances of the GrIS's snow and ice albedo simulations using different snow/ice schemes (BAT, SNICAR-AD and SNCIAR-ADv4), and the amplifying effect of bare ice on the albedo reduction through bare ice-snow-feedback mechanism. However, the 0.5°×0.5° resolution is insufficient to accurately represent the narrow ablation zone, and big resolution gap between MODIS data and the model output is a limitation of this study. In future research, we will study the effects of bare ice albedo changes at a higher resolution to accurately delineate bare ice regions. Future efforts are also needed to consider the actual LACs concentrations within the ice, including BC, dust and snow algae, instead of the equivalent BC, and to investigate its effect on the GrIS's mass loss via land-atmosphere coupling for the land-atmosphere coupling model may produce more pronounced feedback than land-only simulations. Besides, the current methods are still unable to distinguish how the ice density and the size of air bubbles change individually, as the relationship between ice density and the effective radius of air bubbles is arbitrarily prescribed (ρ_{ice}=650 kg.m^{-3} corresponds to R_{eff}=100 µm, ρ_{ice}=916 kg.m^{-3} corresponds to R_{eff}=1500 µm) when constructing the lookup table based on the offline SNICAR-ADv4 model. The precise inversion of ice density and the effective radius of air bubbles within the ice is a scientific problem worthy of further investigation.

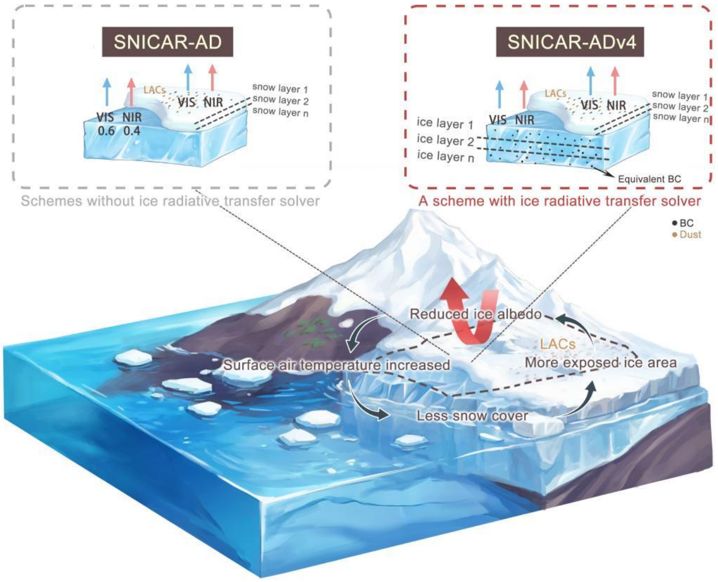

Figure 10. Schematic representation of the snow and land ice column in CoLM BATS, SNICAR-AD and SNICAR-ADv4 (the upper part of the figure), and bare ice-albedo feedback in the GrIS (the lower part of the figure).

Data availability. The SNICAR-ADv4 enabled CoLM2024 code is available on GitHub at https://github.com/guoshuyang23/CoLM-SNICARADv4. The offline SNICAR-ADv4 used in this study can be downloaded at https://github.com/chloewhicker/SNICAR-ADv4. MODIS snow cover data (MOD10C1) used to make the cloud and snow mask for bare ice pixels is available at https://nsidc.org/data/mod10c1/versions/6. MODIS surface reflectance data (MOD09CMG) used to retrieve the bare ice properties is from https://doi.org/10.5067/MODIS/MOD09CMG.061. MODIS surface albedo data (MCD43C3) used to evaluate the simulations and retrieve the bare ice properties is from https://doi.org/10.5067/MODIS/MCD43C3.061

Author contributions. SYG designed the study and wrote the paper. YJD was responsible for to conceptualization, supervision, and funding acquisition. HY contributed to revisions of the manuscript. HBL provided technical support.

Competing interests. The contact author has declared that neither they nor their co-authors have any competing interests.

Acknowledgements. We thank Chloe A. Whicker for sharing the method for processing ice optical property files in the offline SNICAR-ADv4 for use in land surface models.

Financial support. This research was funded by the Guangdong Major Project of Basic and Applied Basic Research (2021B0301030007), the Natural Science Foundation of China (under Grants 42075160, 41730962 and 42088101), the National Key R&D Program of China (under Grant 2017YFA0604300), the Innovation Group Project of Southern Marine Science and Engineering Guangdong Laboratory (Zhuhai) (311021009), and the specific research fund of the Innovation Platform for Academicians of Hainan Province (YSPTZX202143).

References

Abolafia-Rosenzweig, R., He, C., McKenzie Skiles, S., Chen, F., and Gochis, D.: Evaluation and optimization of snow albedo scheme in Noah-MP land surface model using in situ spectral observations in the Colorado Rockies, J. Adv. Model. Earth Syst., 14, e2022MS003141, https://doi. org/10.1029/2022MS003141, 2022.

Alexander, P. M., Tedesco, M., Fettweis, X., van de Wal, R. S. W., Smeets, C. J. P. P., and van den Broeke, M. R.: Assessing spatio-temporal variability and trends in modelled and measured Greenland ice sheet albedo (2000–2013), The Cryosphere, 8(6), 2293–2312, https://doi.org/10. 5194/tc-8-2293-2014, 2014.

Antwerpen, R., Tedesco, M., Fettweis, X., Alexander, P.,and vandeBerg, W. J.: Assessing bare-ice albedo simulated byMAR overthe Greenland icesheet(2000–2021) andimplications formeltwater production estimates, The Cryosphere, 16(10), 4185–4199, https://doi.org/10. 5194/tc-16-4185-2022, 2022.

Box, J. E., Fettweis, X., Stroeve, J. C., Tedesco, M., Hall, D. K., and Steffen, K.: Greenland ice sheet albedo feedback: Thermodynamics and atmospheric drivers, The Cryosphere, 6(4), 821–839, https://doi.org/10.5194/tc-6-821-2012, 2012.

Briegleb, B. P. and Light, B.: A Delta-Eddington multiple scattering parameterization for solar radiation in the sea ice component of the Community Climate System Model, NCAR/TN472+STR, National Center for Atmospheric Research, 108 pp., https://doi.org/10.5065/D6B27S71, 2007.

Chen, X., Zhang, X. , Church, J. A., Watson, C. S., King, M. A., Monselesan, D., Legresy, B., and Harig C.: The increasing rate of global mean sea-level rise during 1993-2014, Nat. Clim. Change,7, 492–495, https://doi.org/10.1038/nclimate3325, 2017.

Chevrollier, L. A., Cook, J. M., Halbach, L., Jakobsen, H., Benning, L. G., Anesio, A. M., and Tranter, M.: Light absorption and albedo reduction by pigmented microalgae on snow and ice, J. Glaciol., 69(274), 333–341. https://doi.org/10.1017/jog.2022.64, 2023.

Cogley, J. G., Hock, R., Rasmussen, L. A., Arendt, A. A., Bauder, A., Braithwaite, R. J., Jansson, P., Kaser, G., Möller, M., Nicholson, L.: Glossary of glacier mass balance and related terms (p. 86), IHP-VII Technical Documents in Hydrology No, 2011.

Cook, J. M., Tedstone, A. J., Williamson, C., McCutcheon, J., Hodson, A. J., Dayal, A., Skiles, M., Hofer, S., Bryant, R., McAree, O., McGonigle, A., Ryan, J., Anesio, A. M., Irvine-Fynn, T. D. L., Hubbard, A., Hanna, E., Flanner, M., Mayanna, S., Benning, L. G., van As, D., Yallop, M., McQuaid, J. B., Gribbin, T., and Tranter, M.: Glacier algae accelerate melt rates on the south-western Greenland Ice Sheet, The Cryosphere, 14, 309330, https://doi.org/10.5194/tc-14-309-2020, 2020.

Danabasoglu, G., Lamarque, J. F., Bacmeister, J., Bailey, D. A., DuVivier, A. K., Edwards, J., Emmons, L. K., Fasullo, J. T., Garcia, R., Gettelman, A., Hannay, C., Holland, M. M., Large, W. G., Lauritzen, P., Lawrence, D. M., Lenaerts-Jan T. M., Lindsay, K., Lipscomb, W. H, Mills, M. J., Neale, R., Oleson, K., Otto-Bliesner, B., Phillips, A. S., Sacks, W. J., Tilmes, S., van Kampenhout, L., Vertenstein, M., Bertini, A., Dennis, J., Deser, C., Fischer, C., Fox-Kemper, B., Elizabeth-Kay, J., Kinnison, D., Kushner, P., Larson, V. E., Long, M., Mickelson, S., Moore, J. K., Nienhouse, E., Polvani, L., Rasch, P. J., and Strand, W. G..: The community Earth system model version 2 (CESM2), J. Adv. Model. Earth Syst., 12, https://doi.org/10.1029/2019MS001916, 2020.

Dang, C., Zender, C. S., and Flanner, M. G.: Intercomparison and improvement of two-stream shortwave radiative transfer schemes in Earth system models for a unified treatment of cryospheric surfaces, The Cryosphere, 13(9), 2325–2343. https://doi.org/10.5194/tc-13-2325-2019, 2019.

Dickinson, R. E., Henderson-Sellers, A., and Kennedy, P. J.: Biosphere-atmosphere transfer scheme (BATS) for the NCAR community climate model (NCAR Tech. Note NCAR/TN-38+STR, Vol. 82), National Center for Atmospheric Research, 1986

Feng, S., Cook, J. M., Naegeli, K., Anesio, A. M., Benning, L. G., and Tranter, M.: The impact of bare ice duration and geo-topographical factors on the darkening of the Greenland Ice Sheet, Geophys. Res. Lett., 51, e2023GL104894, https://doi. org/10.1029/2023GL104894, 2024.

Flanner, M. G., and Zender, C. S. Linking snowpack microphysics and albedo evolution, J. Geophys. Res., 111(D12), https://doi.org/10.1029/2005JD006834, 2006.

Flanner, M. G., Arnheim, J. B., Cook, J. M., Dang, C., He, C., Huang, X., Singh, D., Skiles, S. M., Whicker, C. A., and Zender, C. S.: SNICAR-ADv3: a community tool for modeling spectral snow albedo, Geosci. Model Dev., 14, 7673 – 7704, https://doi.org/10.5194/gmd-14-7673-2021, 2021.

Flanner, M. G., Liu, X., Zhou, C., Penner, J. E., and Jiao, C.: Enhanced solar energy absorption by internally-mixed black carbon in snow grains, Atmos. Chem. Phys., 12(10), 4699–4721, https://doi.org/10.5194/acp-12-4699-2012, 2012.

Flanner, M. G., Zender, C. S., Randerson, J. T., and Rasch, P. J.: Present-day climate forcing and response from black carbon in snow. J. Geophys. Res., 112(D11). https://doi.org/10.1029/2006jd008003, 2007.

Friedl, M.A., Sulla-Menashe, D., Tan, B., Schneider, A., Ramankutty, N., Sibley, A., and Huang X.: Modis collection 5 global land cover: algorithm refinements and characterization of new datasets. Remote Sens. Environ, 114(1), 168–182, https://doi.org/10.1016/j.rse.2009.08.016, 2010

Gardner, A. S., and Sharp, M. J.: A review of snow and ice albedo and the development of a new physically based broadband albedo parameterization, J. Geophys. Res., 115(F1), F01009, https://doi.org/10.1029/2009JF001444, 2010.

Hao, D., Bisht, G., Rittger, K., Bair, E., He, C., Huang, H., Dang, C., Stillinger, T., Gu., Y., Wang, H., Qian, Y., Leung, L. R.: Improving snow albedo modeling in the E3SM land model (version 2.0) and assessing its impacts on snow and surface fluxes over the Tibetan Plateau, Geosci. Model Dev., 16(1), 75–94, https://doi.org/10.5194/gmd-16-75-2023, 2023.

He, C., and Flanner, M.: Snow albedo and radiative transfer: Theory, modeling, and parameterization. In Springer series in light scattering (pp. 67–133), Springer, 2020.

He, C., Flanner, M. G., Chen, F., Bariage, M., Liou, K. N., Kang, S., Ming, J., and Qian, Y.:

Black carbon-induced snow albedo reduction over the Tibetan Plateau: Uncertainties from snow grain shape and aerosol–snow mixing state based on an updated SNICAR model, Atmos. Chem. Phys., 18, 11507–11527, https://doi.org/10.5194/ACP-18-11507-2018, 2018.

He, C., Flanner, M., Lawrence, D. M., and Gu, Y.: New features and enhancements in community land model (CLM5) snow albedo modeling: Description, sensitivity, and evaluation, J. Adv. Model. Earth Syst., 16, e2023MS003861, https://doi.org/10.1029/2023MS003861, 2024.

He, C., Liou, K. N., Takano, Y., Chen, F., and Barlage, M.: Enhanced snow absorption and albedo reduction by dust-snow internal mixing: Modeling and parameterization, J. Adv. Model. Earth Syst., 11(11), 3755–3776, https://doi.org/10.1029/2019ms001737, 2019.

He, C., Takano, Y., Liou, K. N., Yang, P., Li, Q., and Chen, F.: Impact of snow grain shape and black carbon–snow internal mixing on snow optical properties: Parameterizations for climate models, Journal of Climate, 30(24), 10019–10036, https://doi.org/10.1175/jcli-d-17-0300.1, 2017.

Hofer, S., Tedstone, A. J., Fettweis, X. and Bamber, J. L.: Decreasing cloud cover drives the recent mass loss on the Greenland Ice Sheet, Sci. Adv., 3, e1700584, https://doi.org/10.1126/sciadv.1700584, 2017.

King, M. D., Howat, I. M., Candela, S. G., Noh, M. J., Jeong, S., Noël, B. P. Y., Van den Broeke, M. R., Wouters, B., and Negrete, A.: Dynamic ice loss from the Greenland Ice Sheet driven by sustained glacier retreat, Commun. Earth Environ., 1(1), 1. https://doi.org/10.1038/s43247-020-0001-2, 2020.

Kochtitzky, W., Copland, L., King, M., Hugonnet, R., Jiskoot, H., Morlighem, M., Millan, R., Khan, S. A., and Noël, B.: Closing Greenland's mass balance: Frontal ablation of every Greenlandic glacier from 2000 to 2020, Geophys. Res. Lett., 50, e2023GL104095, https://doi. org/10.1029/2023GL104095, 2023.

Li, Y., Yang, K., Gao, S., Smith, L.C., Fettweis, X., and Li, M.: Surface meltwater runoff routing through a coupled supraglacial-proglacial drainage system, Inglefield Land, northwest Greenland, Int. J. Appl. Earth. Obs, Geoinf, p. 106. https://doi.org/10.1016/j.jprocont.2022.08.003, 2022.

Mouginot, J., Rignot, E., Bjørk, A. A., van den Broeke, M., Millan, R., Morlighem, M., Noël, B., Scheuchl, B., and Wood, M.: Forty-six years of Greenland Ice Sheet mass balance from 1972 to 2018, P. Natl. Acad. Sci., 116, 9239–9244, https://doi.org/10.1073/pnas.1904242116, 2019.

Mullen, P. C., and Warren, S. G.:. Theory of the optical properties of lake ice, J. Geophys. Res., 93(D7), 8403–8414, https:// doi.org/10.1029/JD093iD07p08403, 1988.

Naegeli, K., Damm, A., Huss, M., Wulf, H., Schaepman, M., and Hoelzle, M.: Cross-Comparison of albedo products for glacier surfaces derived from airborne and satellite (Sentinel-2 and Landsat 8) optical data, Remote Sens., 9(2), 110. https://doi.org/10.3390/ rs9020110, 2017.

Nolin, A.W., and Stroeve, J.: The changing albedo of the Greenland ice sheet: implications for climate modeling, Ann. Glaciol., 25, 51–57. https://doi. org/10.1017/s0260305500013793, 1997.

Picard, G., Libois, Q., and Arnaud, L.: Refinement of the ice ab-sorption spectrum in the visible using radiance profile measurements in Antarctic snow, The Cryosphere, 10(6), 2655–2672, https://doi.org/10.5194/tc-10-2655-2016, 2016

Ryan, J. C.: Contribution of surface and cloud radiative feedbacks to Greenland Ice Sheet meltwater production during 2002-2023, Commun. Earth Environ., 5(538), https://doi.org/10.1038/s43247-024-01714-y, 2024.

Ryan, J. C., Smith, L. C., van As, D., Cooley, S. W., Cooper, M. G., Pitcher, L. H., and Hubbard, A.: Greenland Ice Sheet surface melt amplified by snowline migration and bare ice exposure, Sci. Adv., 5(3), eaav3738, https://doi.org/10.1126/sciadv.aav3738, 2019.

Sasgen, I., Wouters, B., Gardner, A.S., King, M.D., Tedesco, M., Landerer, F.W., Dahle, C., Save, H., and Fettweis, X.: Return to rapid ice loss in Greenland and record loss in 2019 detected by the GRACE-FO satellites, Commun. Earth Environ, 1, 1-8. https://doi.org/10.1038/s43247-020-0010-1, 2020.

Schaaf, C., Wang, Z., and Strahler, A. H.: Commentary on Wang and Zender-MODIS snow albedo bias at high solar zenith angles relative to theory and to in situ observations in Greenland, Remote. Sens. Environ., 115, 1296 – 1300, https://doi.org/10.1016/j.rse.2011.01.002, 2011.

Schaaf, C., and Wang, Z.: MODIS/Terra+Aqua BRDF/Albedo Albedo Daily L3 Global 0.05Deg CMG V061 [Dataset]. NASA EOSDIS Land Processes DAAC, https://doi.org/10.5067/MODIS/MCD43C3.06, 2021.1

Schneider, A., Flanner, M., De Roo, R., and Adolph, A.: Monitoring of snow surface near-infrared bidirectional reflectance factors with added light-absorbing particles. The Cryosphere, 13(6), 1753–1766, https://doi.org/10.5194/tc-13-1753-2019, 2019

Schneider, A., Zender, C., Loeb, N., and Price, S.: Useofshallow icecoremeasurements toevaluate andconstrain 1980–1990 global reanalyses oficesheetprecipitation rates. Geophys. Res. Lett., 50(19), e2023GL103943, https://doi.org/10.1029/2023GL103943, 2023

Shimada, R., Takeuchi, N., and Aoki, T.: Inter-annual and geographical variations in the extent of bare ice and dark ice on the Greenland ice sheet derived from MODIS satellite images, Front Earth Sci., 4, 43, https://doi.org/10.3389/feart.2016.00043, 2016.

Stibal, M., Box, J. E., Cameron, K. A., Langen, P. L., Yallop, M. L., Mottram, R. H., Khan, A. L., Molotch, N. P., Chrismas, N. A. M., Quaglia, F. C., Remias, D., Smeets, P., Van den Broeke, M. R., and Ryan, J.: Algae drive enhanced darkening of bare ice on the Greenland ice sheet, Geophys. Res. Lett., 44(22), 11463–11471, https://doi.org/10.1002/2017GL075958, 2017.

Stroeve, J., Box, J. E., Gao, F., Liang, S., Nolin, A., and Schaaf, C.: Accuracy assessment of the MODIS 16-day albedo product for snow: Comparisons with Greenland in situ measurements, Remote. Sens. Environ., 94(1), 46–60. https://doi.org/10.1016/j.rse.2004.09.001, 2005.

Tedesco, M., Doherty, S., Fettweis, X., Alexander, P., Jeyaratnam, J., and Stroeve, J.: The darkening of the Greenland ice sheet: Trends, drivers, and projections (1981–2100), The Cryosphere, 10(2), 477–496, https://doi.org/10.5194/tc-10-477-2016, 2016.

Tedstone, A. J., Cook, J. M., Williamson, C. J., Hofer, S., McCutcheon, J., Irvine-Fynn, T., Gribbin, T., and Tranter, M.: Algal growth and weathering crust state drive variability in western Greenland Ice Sheet ice albedo, The Cryosphere, 14, 521–538, https://doi.org/10.5194/tc-14-521-2020, 2020.

Tedstone, A. J., Bamber, J. L., Cook, J. M., Williamson, C. J., Fettweis, X., Hodson, A. J., and Tranter, M.: Dark ice dynamics of the south-west Greenland Ice Sheet, The Cryosphere, 11, 24912506, https://doi.org/10.5194/tc-11-2491-2017, 2017.

Toon, O. B., McKay, C. P., Ackerman, T. P., and Santhanam, K.: Rapid calculation of radiative heating rates and photodissocia-tion rates in inhomogeneous multiple scattering atmospheres, J. Geophys. Res., 94(D13), 16287–16301, https://doi.org/10.1029/ jd094id13p16287, 1989.

Urraca, R., Lanconelli, C., and Cappucci, F.: Gobron, N. Comparison of Long-Term Albedo Products against Spatially Representative Stations over Snow, Remote Sens., 14, 3745. https://doi.org/ 10.3390/rs14153745, 2022.

van den Broeke, Box, J., Fettweis, X., Hanna, E., Noël, B., Tedesco, M., van As, D., van de Berg, W. J., and van Kampenhout, L.: Greenland Ice Sheet Surface Mass Loss: Recent Developments in Observation and Modeling, Curr. Clim. Change Rep., 3, 345356, https://doi.org/10.1007/s40641-017-0084-8, 2017.

Vermote, E.: MODIS/Terra Surface Reflectance Daily L3 Global 0.05Deg CMG V061 [Data set]. NASA EOSDIS Land Processes Distributed Active Archive Center, https://doi.org/10.5067/MODIS/MOD09CMG.061. 2021.

Warren, S. G., and Wiscombe, W. J.:. A model for the spectral albedo of snow. II: Snow containing atmospheric aerosols, J. Atmos. Sci., 37(12), 2734–2745, https://doi.org/10.1175/1520-0469(1980)037<2734:amftsa>2.0.co;2, 1980.

Whicker, C. A., Antwerpen, R., Flanner, M. G., Schneider, A., Tedesco, M., and Zender, C. S.: The effect of physically based ice radiative processes on Greenland ice sheet albedo and surface mass balance in E3SM, J. Geophys. Res.-Atmos., 129, e2023JD040241, https://doi.org/10.1029/ 2023JD040241, 2024.

Whicker, C. A., Flanner, M. G., Dang, C., Zender, C. S., Cook, J. M., and Gardner, A. S.: SNICAR-ADv4: A physically based radiative transfer model to represent the spectral albedo of glacier ice, The Cryosphere, 16(4), 1197–1220, https://doi.org/10.5194/tc-16-1197-2022, 2022.

Williamson, C. J., Anesio, A. M., Cook, J., Tedstone, A., Poniecka, E., Holland, A., Fagan, D., Tranter, M., and Yallop, M.: Ice algal bloom development on the surface of the Greenland Ice Sheet, FEMS Microbiol. Ecol., 94(3), https://doi.org/10.1093/femsec/fiy025, 2018.

Wiscombe, W. J., and Warren, S. G.: A model for the spectral albedo of snow. I: Pure snow. J. Atmos. Sci., 37(12), 2712–2733. https://doi.org/10.1175/1520-0469(1980)037<2712:amftsa>2.0.co;2, 1980.

Ye, F., Cheng, Q., Hao, W., Yu, D., Ma, C., Liang, D., and Shen, H.: Reconstructing daily snow and ice albedo series for Greenland by coupling spatiotemporal and physics-informed models, Int. J. Appl. Earth Obs., 124, 103519, https://doi.org/10.1016/j.jag.2023.103519, 2023.